Complex Resistivity Spectra and the Shear Modulus of the Vortex Solid in Untwinned $YBa_2Cu_3O_7$

Hui Wu* and N. P. Ong
Joseph Henry Laboratories of Physics, Princeton University, Princeton, New Jersey 08544

R. Gagnon and L. Taillefer
Department of Physics, McGill University, 3600 University Street, Montréal, Quebec, Canada H3A 2T8
(Received 28 May 1996)

The complex resistivity $\hat{\rho}$ of the vortex system in $YBa_2Cu_3O_7$ has been measured from 0.2 to 20 MHz. The solid phase below the transition field H_m is characterized by strong dispersion in $\hat{\rho}$. At the transition, an abrupt decrease of the reactance Im $\hat{\rho}$ is observed. We show that this is caused by a collapse of the shear modulus c_{66} at H_m. The experiment provides firm evidence for a first-order melting transition. [S0031-9007(96)02141-2]

PACS numbers: 74.60.Ge, 72.15.Gd, 74.72.Bk

There is now significant evidence that the vortex system in twin-free crystals of the cuprate superconductor $YBa_2Cu_3O_7$ (YBCO) undergoes an abrupt change of state when a transition line H_m is crossed. The transition has been investigated by torque magnetometry [1], flux-flow resistivity [2,3], and detection of the washboard frequency [4]. Most investigators identify the transition as a first-order melting of the vortex solid. However, there is lacking direct evidence for a collapse of the shear rigidity, which is the key feature of a first-order solid-to-liquid transition. Competing scenarios unrelated to melting, such as a dynamic depinning transition [5], have also been proposed.

To probe the rigidity of the vortex solid, we have measured its linear response to a driving current versus frequency. When the lattice is pinned at only a *small* number of sites, the velocity amplitude is determined by competition between the shear rigidity and the damping force. At low frequencies, the former dominates, and the response is weak and out of phase with the driving force. At high frequencies, however, the opposite is true, and the velocity is large and in phase. The crossover (at the "shearing" frequency) occurs when the two forces are comparable. Thus, the spectrum of the velocity response allows the shear rigidity to be found. By measuring the complex spectra at several field values, we have used this method to determine how the shear modulus changes across H_m.

Crystals of optimally doped $YBa_2Cu_3O_7$ with a critical temperature $T_c = 93.5$ K were detwinned by application of uniaxial stress. Low-impedance contacts (100 mΩ) were made with silver epoxy. The small impedance of YBCO crystals ($\leq$10 mΩ) poses difficult problems for high-frequency measurements. To measure the complex resistivity $\hat{\rho} = \rho_1 + j\rho_2$ to sufficient accuracy, we have modified a scattering technique [6] to study low-impedance samples for frequencies $\omega/2\pi$ up to 20 MHz [7]. The sample impedance is determined by phase detection of the transmitted waves using a high-frequency lock-in amplifier (Palo Alto Research Model 100) (details will be given in Wu *et al.* [7]). In all measurements, the current amplitude is kept sufficiently low to stay within linear response, and the skin depth is larger than the crystal thickness.

In agreement with earlier work [2–4], we observe an abrupt increase in the dc resistivity in the vortex state when the transition field H_m is exceeded [broken line in Fig. 1(a)]. For fields less than H_m the dc resistivity is below our resolution ($\leq 1\ \mu\Omega$ cm). However, in a high-frequency current the dissipative part ρ_1 becomes finite even in weak fields (see trace at 0.2 MHz). At all fields below H_m, ρ_1 displays a strong dependence on frequency and H. By contrast, above H_m, the ω dependence is much weaker: increasing ω by two decades changes ρ_1 by less than 20%. The reactive component ρ_2 also shows strong frequency dependence below H_m [Fig. 1(b)]. We have plotted the effective inductance $\mathcal{L}$, defined as ρ_2/ω, to display the dispersion more clearly. As a function of field, $\mathcal{L}$ initially increases rapidly with a slope that varies roughly logarithmically with ω. At the transition, $\mathcal{L}$ undergoes a sharp collapse (this remarkable jump is absent in thin-film samples [6,8,9]). Again, above H_m, both the frequency and field dependences are considerably weaker.

A complementary way to display the data is to plot the frequency dependence of $\hat{\rho}$ with H fixed. In fields below H_m, ρ_1 increases monotonically with ω [Fig. 2(a)]. With increasing field (1.0 to 2.5 T), the negative curvature in ρ_1 becomes more pronounced, especially at low frequencies. As the field approaches the melting field, the increase in ρ_1 becomes very rapid, rising to 3 mΩ in less than 1 MHz (see curves at 4.0 and 4.1 T). This remarkable increase in ρ_1 with ω, signalling rapid changes in the lattice just below H_m, abruptly disappears above H_m. In the liquid phase, the frequency dependence of ρ_1 is much weaker (the spectrum is approximately the sum of a large

 0031-9007/97/78(2)/334(4)$10.00

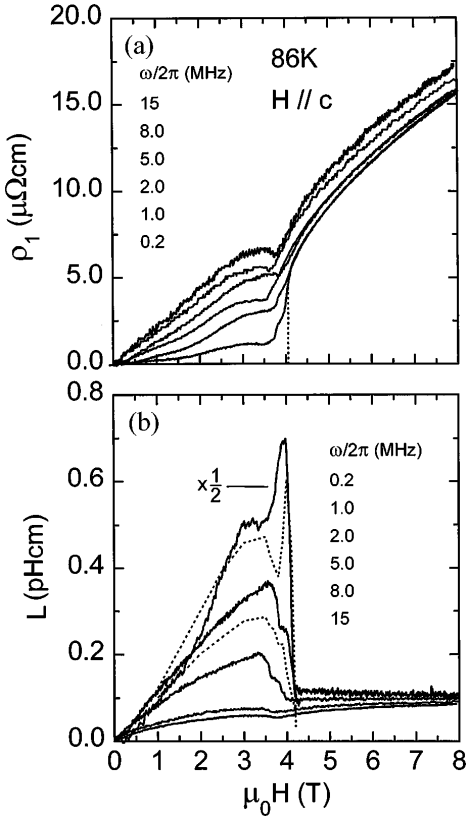

FIG. 1. (a) The field dependence of $\rho_1 \equiv \mathrm{Re}\ \hat{\rho}$ in YBCO at fixed ω, with $\mathbf{H} \parallel \mathbf{c}$ (ω increases from bottom curve to top). The dc resistivity (dashed line) increases abruptly at the transition field H_m. The dispersion is much stronger below H_m compared with above. (b) Shows the corresponding behavior of the inductance $\mathcal{L} \equiv \mathrm{Im}\ \dot{\rho}/\omega$ (ω increases from top curve to bottom). At the transition field, $\mathcal{L}$ undergoes an abrupt collapse as the vortex system enters the liquid state. Broken lines (at 0.2 and 1.0 MHz) are the inductance calculated using parameters derived from fits to ρ_1 (curves at 0.2 MHz have been reduced by 0.5).

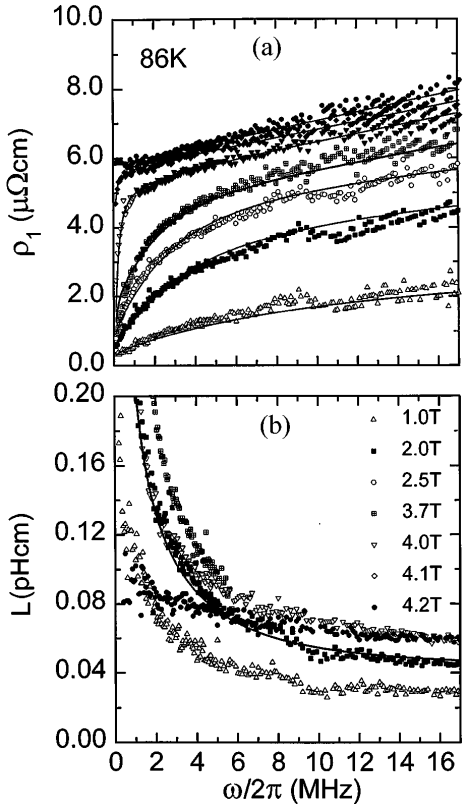

FIG. 2. (a) The spectrum of ρ_1 measured in fixed field ($\mathbf{H} \parallel c$) at 86 K. Field values associated with symbols are given in (b). As $H \rightarrow H_m$ from below, the negative curvature becomes increasingly pronounced (but ρ_1 vanishes at $\omega = 0$). Above H_m, however, ρ_1 is only weakly ω dependent, and attains a large finite value at $\omega = 0$. Solid lines are fits to the model. For the curve at 2.5 T, we used $c_{66} = 280\ \mathrm{J/m^3}$, $\omega_p/2\pi = 61.2$ MHz, and $\eta = 1.13 \times 10^{-7}\ \mathrm{Ns/m^2}$. (b) Shows the spectra of $\mathcal{L}$. The low frequency divergence abruptly disappears when H_m is exceeded (4.0 and 4.2 T). Solid line is calculated from parameters derived from fit to ρ_1 at 2 T (an ω-independent background is included).

constant term and a weak ω-linear term). Similar changes are observed in the inductance [Fig. 2(b)]. In the solid phase $\mathcal{L}$ diverges strongly as ω decreases (curves at 2 and 4 T). However, above H_m, this divergence disappears (curve at 4.2 T). As may be seen by comparison with Fig. 1(b), the sudden disappearance corresponds to the abrupt collapse of $\mathcal{L}$ at H_m.

The spectra in Figs. 1 and 2 uncover significant changes that unfold at lower and lower frequency scales as H approaches H_m from below. Above H_m, however, the spectra are relatively featureless. The abrupt change in the frequency response as the field crosses H_m is specific to untwinned crystals. We note especially the steep rise in ρ_1 at low frequencies just below H_m [Fig. 2(a)], and the collapse of $\mathcal{L}$ at H_m [Fig. 1(b)]. These are not observed in thin-film YBCO [6,8,9].

We will focus mainly on these large changes and argue, with the help of a simple model [10], that they result from the collapse of the shear modulus. We sketch the main ideas. The applied supercurrent $\mathbf{J}e^{j\omega \mathbf{t}}$ exerts a Lorentz force $\mathbf{J} \times \mathbf{B}$ on a vortex (located, say, at site $\mathbf{l}$ of a hexagonal lattice). The displacement amplitude $\mathbf{u}_l$ is determined by competition between the viscous damping force (proportional to ω) and elastic forces generated by the displacement $\mathbf{u_m}$ of its neighbors, as expressed by the elastic force matrix $\mathbf{D}(\mathbf{l}, \mathbf{m})$. In addition, nearby pins may exert a restoring force. However, to account for the rapid changes in the spectra, we assume that the average separation of pinning centers R_0 is much larger than the vortex spacing. A relatively small number of vortices N_{pin} (at pin sites $\mathbf{i}$) experience directly the pinning force $-\kappa \mathbf{u_i}$ (κ is the Labusch parameter). The remaining vortices sense the pinning force via the elastic force matrix. The transmission of these forces may be characterized by an ω-dependent range R_G, which may be derived by balancing the elastic force against the damping force $-\eta \dot{\mathbf{u}}_\mathbf{l}$ (η is the drag viscosity). We find that

$R_G = \sqrt{c_{66}a^2/\eta\omega}$, where c_{66} is the shear modulus and a^2 is the area occupied by a flux quantum Φ_0.

At low ω, the range R_G is extended (if c_{66} is finite), so that the average vortex is restrained by a large number of pins. The vortex lattice responds to the driving force as a strongly pinned solid with a velocity response that is almost purely inductive. As ω increases, the reduction in the range leads to an increase in the velocity amplitude and a rapid decrease in the inductance, consistent with the curves at 2 T in Fig. 2. At high frequency, R_G eventually becomes shorter than R_0, and a large fraction of the vortices oscillate unhindered by the pins. The dissipation ρ_1 approaches the free-flow value $B\Phi_0/\eta$ while the inductance decreases to $\mathcal{L}_{\rm liq}$. If we raise the field close to H_m, softening of the shear modulus reduces R_G, so that the crossover in ρ_1 occurs at lower frequencies (compare the 2.5 and 4.0 T curves). Finally, in the liquid phase R_G is of the order a, and most of the vortices are decoupled from the pins.

The dependence of R_G on the ratio c_{66}/ω presents a way to probe the rigidity of the lattice over successively longer length scales by decreasing ω. In the solid, increasing the probing length ($\omega \to 0$) always leads to the zero-dissipation state [see Fig. 2(a)]. However, as soon as H_m is exceeded, the state at $\omega = 0$ has a finite dissipation (curve at 4.2 T).

In a simple fluid, we expect the inductance to be vanishingly small and ρ_1 to be large but frequency independent. However, the observed behavior is rather different. As shown in Figs. 1 and 2, the inductance $\mathcal{L}_{\rm liq}$ remains relatively large, while ρ_1 retains a weak ω-linear dependence. The data imply that correlation effects continue to play a role in the vortex liquid. Examination of the 15 MHz curve in Fig. 1(b) shows that, at high frequency, there is almost no distinction between the low-field and high-field response, aside from the slight anomaly at H_m. This suggests that, on short time scales, the velocity amplitude is similar in the two states. Equivalently, the environment around each vortex at short distances is quite similar in the two phases. To distinguish the solid from the liquid it is necessary to go to low frequencies. Thus, in Fig. 2, both ρ_1 and $\mathcal{L}$ at the fields 4.0 and 4.2 T are closely similar except below 2 MHz. These effects are reminiscent of the response observed in complex fluids. The comparison will be discussed elsewhere.

In our simplified model [10], we write the equation of motion as

$$\eta\dot{\mathbf{u}}_\mathbf{l} + \sum_\mathbf{m} \mathbf{D}_{\mathbf{l},\mathbf{m}} \cdot \mathbf{u}_\mathbf{m} + \kappa \sum_\mathbf{i} \mathbf{u}_\mathbf{i}\delta_{\mathbf{l},\mathbf{i}} = \mathbf{J} \times \mathbf{\Phi}_0 . \quad (1)$$

In comparison with single-vortex models [11], Eq. (1) includes explicitly the elastic force term. Moreover, the sum over $\mathbf{i}$ is restricted to $N_{\rm pin}$ pin sites, while the sum over $\mathbf{m}$ extends to all N vortices. The propagation of the restoring force to vortices at remote sites is described by the lattice Green's function

$$G(\mathbf{R},\omega) = \frac{1}{N}\sum_\mathbf{q} \frac{[\hat{\mathbf{y}} \cdot \hat{e}_T(\mathbf{q})]^2 e^{j\mathbf{q}\cdot\mathbf{R}}}{[D_T(\mathbf{q}) + j\omega\eta]} , \quad (2)$$

where only the transverse modes are retained for simplicity. The Fourier transform $D_T(\mathbf{q})$ of the elastic matrix is related [12,13] to the moduli c_{66} and c_{44} by $D_T(\mathbf{q}) = [c_{66}q^2 + c_{44}q_z^2]a^2$, where $q_z = \mathbf{q}\cdot\hat{\mathbf{c}}$ and $q = |\mathbf{q} - q_z\hat{\mathbf{c}}|$. In terms of G, we may write down a mean-field solution of Eq. (1) for the resistivity [10], viz.,

$$\hat{\rho}(\omega) = \left(\frac{B\Phi_0}{\eta}\right)\left(1 - \left(\frac{\kappa N_{\rm pin}}{j\omega\eta N}\right) \times \left\{1 + \frac{\kappa N_{\rm pin}}{j\omega\eta N} + \kappa\left[G(0,\omega) + \sum_\mathbf{i}{}' G(\mathbf{R}_\mathbf{i},\omega)\right]\right\}^{-1}\right). \quad (3)$$

As short-range correlation effects and longitudinal modes have been neglected, the model cannot address the high-frequency background described above. Empirically, however, the background terms vary slowly with respect to field and frequency, and are easily separated from the much larger changes associated with softening of the lattice. An adequate approximation to the background is obtained by adding a term $\hat{\rho}^b = \rho_1^b + j\rho_2^b$ to Eq. (3). Both terms are found to be linear in both ω and H.

In fitting the model to experiment, we find that good fits may be obtained only by taking $c_{44} \ll c_{66}$. In this two-dimensional limit, the curvature of the spectrum of ρ_1 is most sensitive to the shearing frequency $\omega_{66} \equiv (4\pi c_{66}/\eta)(a/R_0)^2$ (we take κ to be field independent). Physically, ω_{66} is the frequency at which the range R_G of $G(R,\omega)$ matches the pin spacing R_0, as discussed earlier. Rather close fits to the data may be achieved (solid lines in Fig. 2). We have used only the ρ_1 data for the fits. The viscosity η, which sets the overall scale of ρ_1, is known independently from the high-frequency response (the free-flow limit). Unfortunately, a simple rescaling of the frequency shows that $\hat{\rho}$ is only weakly dependent on R_0 (as $\log R_0$). As a result, c_{66} may be determined from ω_{66} only to within a constant that depends on R_0. [Nonetheless, we have checked that the fit values for ω_{66} are quite reasonable. If we assume that c_{66} at 1 T is given [14] by $\Phi_0 B/(8\pi\lambda)^2 \sim 420\ \mathrm{J/m^3}$ with the penetration length [15] $\lambda \sim 2800$ Å at 86 K, the value of $\omega_{66}/2\pi$ (340 MHz at 1 T) corresponds to $R_0 \sim 7a = 3200$ Å.]

The field dependence of the shear modulus normalized to its value at 1 T is displayed in Fig. 3. Initially, c_{66} rises slowly between 1 and 2 T. Between 2.5 and 3.6 T, c_{66} remains relatively unchanged. However, further increase in field produces a weak peak at 3.6 T, followed by a dramatic decrease by a factor of 400, as the system crosses the melting line. The collapse of the shear modulus is similar to that observed in crystalline solids and polyball suspensions in electrolytes [16] at their melting

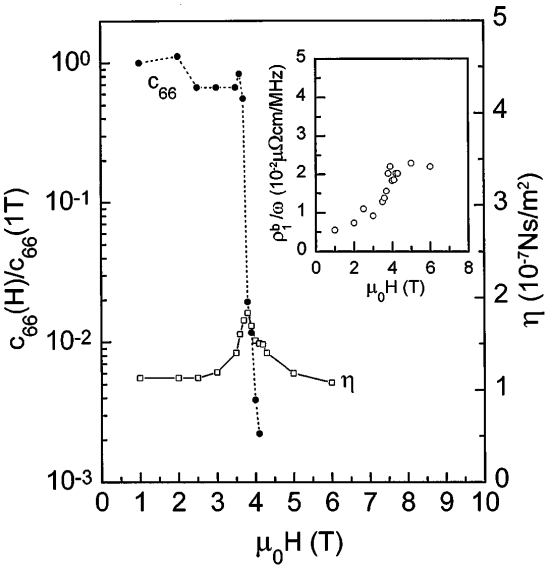

FIG. 3. Field dependence of the shear modulus c_{66} (solid symbols) determined by fitting model to ρ_1 at 86 K (normalized to its value 420 J/m^3 at 1 T). The modulus remains at a plateau value between 2.4 and 3.5 T, then it develops a weak peak near 3.6 T before collapsing by a factor of 400 as H_m is exceeded. The viscosity (open symbols) displays a sharp cusp at H_m (κ is independent of H). The inset shows the field dependence of the background term ρ_1^b/ω used in the fit.

transitions. We regard this collapse to be hard evidence for a first-order transition. The viscosity displays a sharp upward cusp. We do not understand the origin of this cusp, but note that its effect on the high-frequency curve (15 MHz) is quite apparent in Fig. 1(a). The inset shows the field dependence of the ω-linear background term used in the fit to ρ_1.

With the values of ω_{66}, κ and η obtained from fits to ρ_1 at each field, we may calculate the inductance $\mathcal{L}$ as a consistency check. The calculated curves at 0.2 and 1 MHz [broken lines in Fig. 1(b)] capture rather well the observed behavior. The parameters have not been adjusted to refine further the fit to $\mathcal{L}$. However, we have added to the calculated inductance a background term identical to the featureless curve measured at 15 MHz (lowest curve). Initially, $\mathcal{L}$ increases nearly linearly with field with a frequency-dependent slope. In both the simulated and measured curves at 0.2 MHz, $\mathcal{L}$ displays a sharp peak before falling rapidly to the value $\mathcal{L}_{\rm liq}$ as H exceeds H_m (the peak is absent at higher frequencies). The simulation persuades us that the sharp decrease in the inductance is indeed directly related to the collapse in c_{66}. The calculated inductance also describes the observed low-frequency behavior rather well if we include a constant background [solid line in Fig. 2(b)].

In summary, we have shown that the spectra of the complex resistivity provide new information on the transition of the vortex system. We find a dramatic decrease of the characteristic frequency scale as the field approaches H_m. Simultaneously, the resistivity rises very steeply with frequency. At H_m, the low-ω inductance displays an abrupt collapse. These features are consistent with a collapse of the shear modulus at the transition. With a simple model, we have obtained the field dependence of c_{66} and η by fitting to the spectra of ρ_1. We find that c_{66} undergoes a steep decrease of about 400 at H_m. In the analysis, we have neglected short-range correlation effects that are dominant in the liquid (as well as in the solid at high frequencies). These require a more sophisticated treatment.

We acknowledge useful discussions with P. M. Chaikin and D. A. Huse. H. W. and N. P. O. are supported by the U.S. Office of Naval Research (Contract No. N00014-90-J-1013). R. G. and L. T. are funded by NSERC of Canada and FCAR of Quebec. L. T. acknowledges support from the Canadian Institute for Advanced Research and the A. P. Sloan Foundation.

*Present address: Lucent Technologies 1C-119, Bell Innovation Labs., Murray Hill, NJ 07974.

[1] R. G. Beck, D. E. Farrell, J. P. Rice, D. M. Ginsberg, and V. G. Kogan, Phys. Rev. Lett. **68**, 1594 (1992).
[2] H. Safar, P. L. Gammel, D. A. Huse, and D. J. Bishop, Phys. Rev. Lett. **69**, 824 (1992).
[3] W. K. Kwok, J. Fendrich, S. Fleshler, U. Welp, J. Downey, and G. W. Crabtree, Phys. Rev. Lett. **72**, 1092 (1994).
[4] J. M. Harris, N. P. Ong, R. Gagnon, and L. Taillefer, Phys. Rev. Lett. **74**, 3684 (1995).
[5] W. Jiang, N.-C. Yeh, D. W. Reed, U. Kriplani, and F. Holtzberg, Phys. Rev. Lett. **74**, 1438 (1995).
[6] Hui Wu, N. P. Ong, and Y. Q. Li, Phys. Rev. Lett. **71**, 2642 (1993).
[7] Hui Wu, N. P. Ong, R. Gagnon, and L. Taillefer (to be published).
[8] H. K. Olsson, R. H. Koch, W. Eidelloth, and R. P. Robertazzi, Phys. Rev. Lett. **66**, 2661 (1991).
[9] Dong H. Wu, J. C. Booth, and Steven M. Anlage, Phys. Rev. Lett. **75**, 525 (1995).
[10] N. P. Ong and Hui Wu (to be published).
[11] J. I. Gittleman and B. Rosenblum, Phys. Rev. Lett. **16**, 734 (1966); J. Appl. Phys. **30**, 2617 (1968).
[12] L. I. Glazman and A. E. Koshelev, Phys. Rev. B **43**, 2835 (1991).
[13] A. Houghton, R. A. Pelcovits, and A. Sudbo, Phys. Rev. B **40**, 6763 (1989).
[14] V. G. Kogan and L. J. Campbell, Phys. Rev. Lett. **62**, 1552 (1989).
[15] S. D. Kamal *et al.*, Phys. Rev. Lett. **73**, 1845 (1994).
[16] H. M. Lindsay and P. M. Chaikin, J. Phys. (Paris), Colloq. **46**, C3-269 (1985); H. M. Lindsay *et al.*, J. Phys. A **19**, 2583 (1986).